May 2024

Convergence of interference term at next-to-next-to-leading order in Higgs boson to $b\bar{b}$ decay

Cristina Martín-Viveros Díaz-Oliver

Theoretical Particle Physics
Division of Particle and Nuclear Physics
Department of Physics
Lund University

Bachelor thesis (15 hp) supervised by Rikkert Frederix

LUND
UNIVERSITY

Abstract

Higgs boson decay to bottom, anti-bottom quarks is the major decay channel due to the fact that these quarks have a relatively high mass and the Higgs coupling to a particle is proportional to its mass. This process is difficult to detect experimentally because of the jets produced by the quarks. In computations of this decay at next-to-next-to-leading order (NNLO), there is a specific term which has been claimed to be finite on its own and negligible. This term corresponds to the interference between two specific processes, firstly, the Higgs coupling to a top-quark loop, from which two gluons are produced and one of them produces a pair of bottom quarks. The other diagram being Higgs boson decay to bottom anti-bottom quarks, and emission of a gluon from one of these particles. The aim of this paper is twofold: firstly, to show that this term is finite on its own by means of theoretical arguments as well as by analysis of numerical results. Secondly, to check that this term is negligible as it has been claimed.
Analyses of numerical results indicates that the term is finite, but its contribution is bigger than the current theoretical uncertainty. Thus, it is not negligible.

Popular introduction

Particle physics is concerned with the small particles that all things around us are composed of. So, in a sense, it aims to find out what are the Lego bricks building up the universe. This is not an easy task and, for decades, scientists have devoted a lot of time and work to it. For instance, in the 19th century it was believed that the fundamental piece, our Lego brick, if you wish, was the atom. However, later on, when people were shooting things at a thin golden sheet, they found out that that was actually not quite true. In fact, the atom is made up of a positively charged nucleus and negatively charged particles, electrons, going around. Later on, yet again, scientists found out that the nucleus is made up of more fundamental particles - up and down quarks - and up to this point, it has been experimentally shown that these are fundamental particles.

More generally, it has been found that there are a total of 12 fundamental particles which matter consists of also known as fermions, and 5 bosons or force carriers, which act like messengers between the other particles. Understanding how these bosons and fermions interact answers questions like, for example, why most matter around us is made up of only 3 fundamental particles. As it turns out, not all particles are equally long-lived and how long-lived they are can be understood from how they interact. For example, the analogue of the electron, but slightly heavier, is called the muon and it only lives a fraction of a second! Afterwards, the muon decays into an electron and two very light particles known as neutrino.

To calculate how likely a way of decaying is, we normally make use of so-called Feynman diagrams. Feynman diagrams describe interactions through lines and points, where lines represent particles moving in space and points represent the interactions between particles. Counting the number of points in the Feynman diagram gives an idea of how likely the process is. Generally, the more complicated the diagram is the less likely it is that the process occurs.

But, when calculating the likelihood of some slightly more complicated interactions, the probability goes to infinity. This is not very good, but there are some known ways of solving this issue.
In my thesis, I focus on a particular decay of the Higgs boson - this heavy boson gives mass to other particles and decays quickly. More precisely, my thesis studies whether this particular decay is finite and how large it is, compared to the simplest diagram of the decay. In general, understanding these type of slightly-more-complicated diagram helps creating a better understanding of one of the Lego bricks. For my thesis, the Lego brick of interest is the Higgs boson.

Contents

1 Introduction **5**

2 Theory **6**

2.1 Perturbative expansion 6

2.2 On UV and IR divergences 8

2.3 Arguments for convergence 10

3 Methods **11**

4 Results **13**

4.1 On convergence 13

4.2 Size of the contribution 14

4.3 Phase-space analysis 14

4.3.1 Dalitz plot 14

4.3.2 Angular distributions 15

5 Conclusion **17**

Acknowledgements **17**

References **17**

List of Figures

1 The two interference terms at NNLO previously omitted. The diagram on the left interference is denoted as real-virtual interference, and the diagram on the right is known as double-virtual interference. 5

2 Sketch of some of the Feynman diagrams for $H \to b\bar{b}$. The first diagram corresponds to the zeroth order term, the second one contributes to NLO, and the last one is an example of a process contributing to NNLO. 7

3 Sketch of some of the Feynman diagrams for $H \to b\bar{b}g$. The first two diagrams correspond to the zeroth-order terms and the last one is an example of a process at $\alpha_s^{\frac{3}{2}}$. 7

4 Plot showing the theoretical coupling constant and its dependency on the energy scale ($Q = |q|$). The values are taken from measurements at TRISTAN and LEP. The Picture taken from Ref. [10], p.595. 8

5 Virtual-real interference term with labels for each propagator. 10

6 Plot of $f(x) = \sqrt{x}$. 12

7 Feynman diagrams taken from MG showing the relevant couplings for determining the interference of interest. 13
8 Decay width as a function of the ratio of the magnitude of the momentum of g and b. 14
9 Dalitz plot for Higgs boson decay. On the x-axis $m^2_{b\bar{b}}$, on the y-axis $m^2_{g\bar{b}}$ and the colour-bar shows m^2_{bg} in GeV^2. 15
10 Decay width as a function of the angle between b and g in radians. 16
11 Decay width as a function of the angle between g and $\bar{b}$ in radians. 16
12 Histogram showing the angle between b and $\bar{b}$ in radians. 17

List of Symbols and Abbreviations

α_s	Strong coupling constant
$\mathcal{A}$	Amplitude
$\mathcal{M}$	Matrix element
EFT	Effective Field Theory
HEFT	Higgs Effective Field Theory
IR	Infrared
KLN	Kinoshita–Lee–Nauenberg
LO	Leading order
MG	MadGraph5_aMC@NLO
NLO	Next-to-leading order
NNLO	Next-to-leading order
UV	Ultraviolet

1 Introduction

In the 1960s, one of the apparent problems with the Standard Model was that it predicted particles to be massless. The solution to this problem came independently from P. Higgs, F. Englert and R. Brout in 1964 [1], [2], who later won the Nobel prize for the mechanism giving mass to particles in the Standard Model. In this mechanism, later referred to as the Higgs mechanism, particles acquire mass from the interaction with the theorised, and later known as, Higgs boson.
It was not until 2012, though, that the Higgs boson was found at the Large Hadron Collider (LHC) as reported by the CMS and ATLAS collaborations [3], [4], respectively.

Since then, the goal has been shifted towards learning about the Higgs boson's properties in more detail. One relevant aspect to look at is the main decay channel of the Higgs boson to bottom quarks. This decay channel is dominant due to the fact that the coupling of the Higgs boson to particles is proportional to their mass - the top quark, as well as the W, Z bosons being too heavy to be produced by Higgs boson decay. From the experimental point of view, the Higgs boson decay to $b\bar{b}$ is relevant to measure the Yukawa coupling of the Higgs to bottom quarks (Y_b). However, this decay channel is rather difficult to detect experimentally.

Including next-to-leading order (NLO) terms in the calculation of the matrix element has significant impact, whereas for next-to-next-to-leading order (NNLO) the decay rate is changed only slightly with respect to NLO (see, for example, Figure 1 in Ref. [5]). This shows that in order to improve the accuracy of decay rates, couplings, etc., it becomes relevant to include higher order terms (corrections) and it also hints at the fact that there is some convergence of the terms, that is, higher order terms tend to converge to some specific value such that at some point including even higher order corrections does not improve the results significantly.

For Higgs boson decay to bottom, anti-bottom massive quarks, the decay rate is known up to NNLO, that is, α_s^2. However, these computations, such as in Refs.[6], [7], have omitted the interference terms shown in Figure 1, as, according to these authors, the terms are finite and negligible. These interference terms are referred to as real-virtual, Figure 1a, and double virtual, Figure 1b, following the notation introduced in Ref. [8].

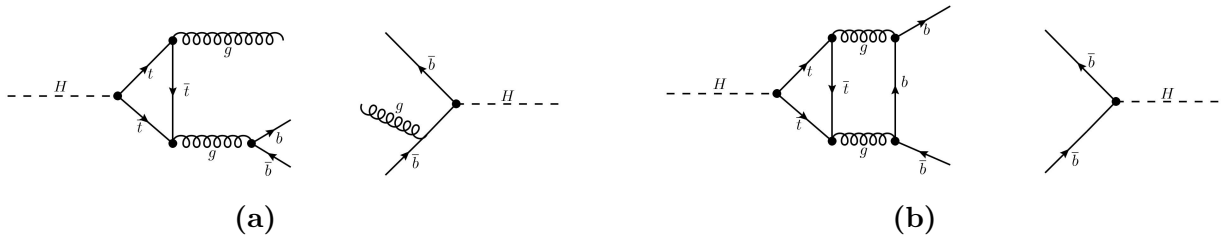

Figure 1: The two interference terms at NNLO previously omitted. The diagram on the left interference is denoted as real-virtual interference, and the diagram on the right is known as double-virtual interference.

Except for Ref. [8], where an analytical formula is given for the matrix element of the interference, the contribution has been previously neglected. In this paper we focus on the contribution given in Figure 1a, referred to as real-virtual interference term in Ref. [8]. In particular, we show that the real-virtual interference term is finite in two ways: firstly, by means of theoretical arguments and, secondly, by simulating the interference

term in MadGraph5_aMC@NLO. Additionally, we compute the value of the contribution and compare it to the leading order to see if it is negligible or not.

The thesis is organised as follows. In section 2, we give some theoretical background, particularly focusing on the perturbative expansion of Higgs decay to $b\bar{b}$ and explaining how this expansion is granted to be free of infrared divergences by the Kinoshita–Lee–Nauenberg theorem. We also give some arguments for why the contribution of interest is finite on its own. In Section 3, we present the syntax for the simulation of Higgs boson decay in MadGraph5_aMC@NLO. In Section 4, we present the analysis of the results showing that the contribution is finite but not negligible. The thesis concludes with Section 5, where we give possible ways of extending this project.

2 Theory

In this section, we discuss the perturbative expansion for $H \to b\bar{b}$. We briefly talk about divergences that appear when finding the matrix element. The section concludes by discussing the convergence of the virtual-real interference term.

2.1 Perturbative expansion

For a general decay, say $A \to B$, the matrix element can be expanded as a power series of the coupling constant relevant for the interaction, α for our example, as shown in the following equation:

$$\mathcal{M}_B = \mathcal{M}_B^{(0)} + \alpha\mathcal{M}_B^{(1)} + \alpha^2\mathcal{M}_B^{(2)} + ..., \tag{1}$$

where the subscript indicates the final product(s). Typically, the total matrix element is not calculated exactly, but instead is approximated to some order, α^n. This is due to the fact that there are many diagrams contributing at high orders, and generally the higher the order the more likely these terms are to be a small contribution to the total expansion - though this only holds if the coupling constant takes a small value in the regime that is being considered. For, say $n = 1$, this approximate element squared is given by

$$\begin{aligned} |\mathcal{M}_B|^2 &= |\mathcal{M}_B^{(0)}|^2 + \alpha^2|\mathcal{M}_B^{(1)}|^2 + \alpha\left[(\mathcal{M}_B^{(0)})^*\mathcal{M}_B^{(1)} + (\mathcal{M}_B^{(1)})^*\mathcal{M}_B^{(0)}\right] \\ &= |\mathcal{M}_B^{(0)}|^2 + 2\alpha\,\mathrm{Re}\Big\{\mathcal{M}_B^{(0)}(\mathcal{M}_B^{(1)})^*\Big\} + \alpha^2|\mathcal{M}_B^{(1)}|^2 \end{aligned} \tag{2}$$

where the first term in Eq.(2) is referred to as leading order (LO), the second term, which corresponds to the interference between $\mathcal{M}_B^{(0)}$ and $\mathcal{M}_B^{(1)}$. This term contributes to as next-to-leading order (NLO), and the third term contributes to next-to-next-to-leading order (NNLO). The same way of naming the terms applies to higher-order terms.

Another relevant point to make is that the power series expansion can be done at the matrix element level, such as in Eq.(1), or at the squared matrix element level, such as the one in Eq.(2). However, it seems more intuitive to expand first at matrix element level to then see where the interference terms come from.

When A can decay to B and also to C, the total matrix element can be obtained as follows:

$$|\mathcal{M}_{TOT.}|^2 = |\mathcal{M}_B|^2 + |\mathcal{M}_C|^2, \tag{3}$$

where $\mathcal{M}_B$ and $\mathcal{M}_C$ are power expansions as shown in Eq.(1). Here we add the squares of the matrix elements because the final products are not the same.

The same power series expansion, as done in Eq.(1), can be performed for $H \to b\bar{b}$. In this case, the coupling constant is α_s, as processes including quarks are more likely to interact via the strong force rather than interacting electromagnetically [1].

$$\mathcal{M}_{b\bar{b}} = \mathcal{M}^{(0)}_{b\bar{b}} + \alpha_s \mathcal{M}^{(1)}_{b\bar{b}} + \alpha_s^2 \mathcal{M}^{(2)}_{b\bar{b}} + ..., \tag{4}$$

In this expansion, the first term corresponds to the Higgs boson decaying to a bottom-anti-bottom quark pair, the second term includes a virtual gluon loop connecting the bottom quark to the anti-bottom quark, and so on. Some terms from this expansion are drawn as Feynman diagrams in Figure 2.

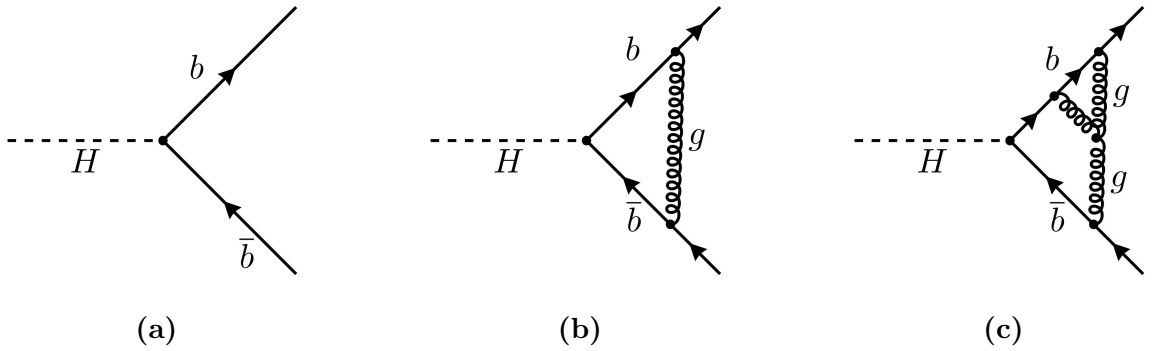

Figure 2: Sketch of some of the Feynman diagrams for $H \to b\bar{b}$. The first diagram corresponds to the zeroth order term, the second one contributes to NLO, and the last one is an example of a process contributing to NNLO.

Figure 2 shows that the LO term, or $\mathcal{M}^{(0)}_{b\bar{b}}$, is a tree-level diagram; NLO terms, $\mathcal{M}^{(1)}_{b\bar{b}}$, in some cases contain a virtual loop; NNLO terms, $\mathcal{M}^{(2)}_{b\bar{b}}$, sometimes contain double virtual loops.

A similar expansion can be done for $H \to b\bar{b}g$.

$$\mathcal{M}_{b\bar{b}g} = \alpha_s^{\frac{1}{2}} \mathcal{M}^{(0)}_{b\bar{b}g} + \alpha_s^{\frac{3}{2}} \mathcal{M}^{(1)}_{b\bar{b}g} + ..., \tag{5}$$

In this case the zeroth order term in the expansion, the coupling constant appears in the square root instead of to the power of zero, as in Eq.(4), because of the additional gluon-bottom quark vertex. Similarly, for the first-order term, since there is a top-quark loop, there are three gluon quark vertices and each vertex amounts to one $g_s = \sqrt{4\pi\alpha_s}$. This is shown in Figure 3b.

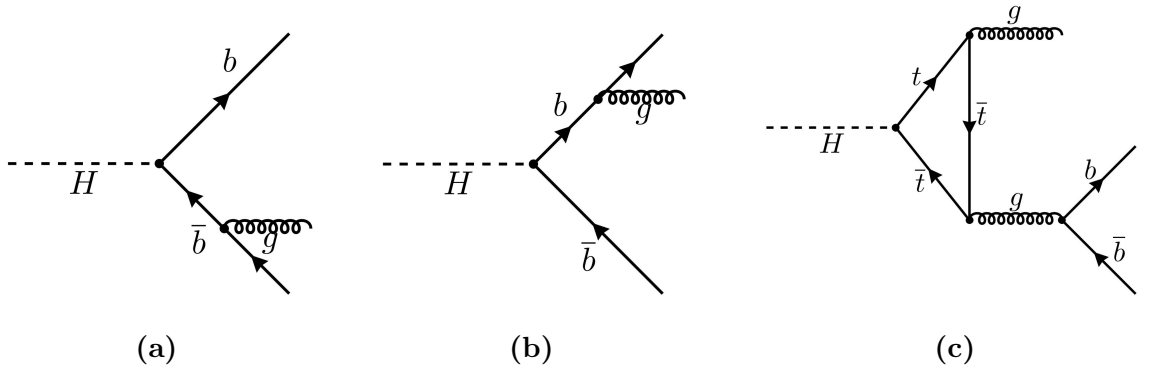

Figure 3: Sketch of some of the Feynman diagrams for $H \to b\bar{b}g$. The first two diagrams correspond to the zeroth-order terms and the last one is an example of a process at $\alpha_s^{\frac{3}{2}}$.

[1] This is because α_s is orders of magnitude greater than the electromagnetic coupling constant.

In the expansion for $H \to b\bar{b}g$, the LO term is still tree-level, and the NLO term sometimes includes loops, as in the case shown in Figure 3c.

For this particular Higgs boson decay, it is also possible to approximate the matrix element by the lowest order (in α_s) terms as the strong coupling constant is rather small at high energies. This can be seen from the running of the strong coupling constant. In particular, its dependence on the energy transfer q^2 is given by (See Ref. [9]):

$$\alpha_s(|q^2|) = \frac{\alpha_s(\mu^2)}{1 + (\alpha_s(\mu^2)/12\pi)(11n - 2f)\ln(|q^2|/\mu^2)},$$

where n is the number of colours, and f the number of flavours. Or graphically in Figure 4, we see that the coupling constant is close to 0.1 for energy transfer close to the Higgs mass, namely 125 GeV.

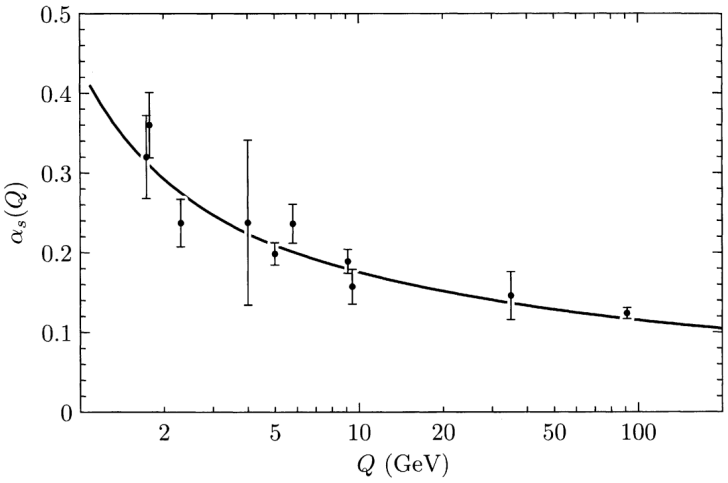

Figure 4: Plot showing the theoretical coupling constant and its dependency on the energy scale ($Q = |q|$). The values are taken from measurements at TRISTAN and LEP. The Picture taken from Ref. [10], p.595.

From this, we can conclude that at high energies, or small distances, the coupling is small such that it does not affect the validity of the matrix element expansion done previously.

2.2 On UV and IR divergences

In diagrams containing virtual loops, such as the one in Figure 2b, there are no restrictions on the virtual particle's momentum [11]. This implies that when calculating the matrix element, the virtual particle's momentum must be integrated over all possible momenta. In these cases, the matrix element is proportional to the following integral (due to the propagators):

$$\mathcal{M} \propto \int \frac{\mathrm{d}^4 k}{k^4},$$

which diverges logarithmically for high momenta. This is known as a Ultraviolet (UV) divergence. This type of divergence is solved by various regularisation schemes, such as dimensional regularisation. Dimensional regularisation makes the integral finite by introducing a dependence on the energy scale and reducing the number of dimensions to $4 - \epsilon$ dimensions. To make the result physically meaningful, the general procedure is to

renormalise and, in doing so, the dependence on ϵ disappears, at least for renormalisable theories such as QCD.

The opposite type of divergences, Infrared (IR) divergences, result from considering the low energy regime. These divergences appear in cases where a massless particle is emitted at very low energy or when it is emitted collinear to the particle that emits it.
This is the case for Higgs boson decay. More precisely, $H \to b\bar{b}$ includes UV divergences because of the virtual gluon loop at NLO, as shown in Figure 2 and $H \to b\bar{b}g$ contains IR divergences due to the real gluon being emitted from the bottom quark or anti-bottom quark. Mathematically, the latter type of divergence can be seen by looking at the bottom quark propagator:

$$i\mathcal{A} \propto \frac{i}{q'^2 - m^2} = \frac{i}{(p_g + p_b)^2 - m_b^2}, \tag{6}$$

where p_g is the 4-momentum of the gluon, p_b is the 4-momentum of the bottom quark, and m_b is the mass of the bottom quark. Expanding the denominator as follows:

$$\begin{aligned}(p_g + p_b)^2 - m_b^2 &= \overset{0}{\cancel{p_g^2}} + \cancel{p_b^2} + 2p_g \cdot p_b - \cancel{m_b^2} \\ &= 2(E_b E_g - \vec{p_b} \cdot \vec{p_g}) \\ &= 2(E_b E_g - E_g\sqrt{E_b^2 - m_b^2}\cos\theta_{b,g}) \\ &= 2E_b E_g \left(1 - \sqrt{1 - \frac{m_b^2}{E_b^2}}\cos\theta_{b,g}\right).\end{aligned} \tag{7}$$

Eq. (7) shows that the denominator can go to zero if the gluon's energy goes to zero, soft divergence, or if the angle between the gluon and bottom quark goes to zero for massless quarks, collinear divergence. In this thesis, quarks are massive, so the focus is on soft divergences.

In the following, we show why this type of divergence could appear and how to solve them in the general case. IR divergences arise from the experimental fact that a quark with a soft, or collinear, gluon cannot be distinguished from a single quark without a gluon. Similarly, for the case of the emission of a multiple soft, or collinear, gluons, the experimental signature would be a single jet. Thus, in this case, the emission of one, or several, soft collinear gluon(s) is indistinguishable from a single quark. Therefore, we see that from the point of view of the observables or experimental signature, a quark emitting a soft, or collinear, gluon is a degenerate state of a single quark without any gluon.

Putting it differently, in Quantum Field Theory energy levels are characterised by the number of particles occupying such state (see Ref. [12], p.54), and here we see that this is no longer the case because a single quark and a quark with a collinear gluon are, in fact, degenerate states, even though the number of particles is different in each case. One way to argue, given in Ref. [13], p.338, is that the soft gluon loses "its particle nature", leading to this characterisation of energy states being insufficient. This means that, ultimately, we are not including all the relevant diagrams. This is the cause for the appearance of IR divergences.

The cancellation of this type of divergence is done by including all final and initial degenerate states, and, formally, the convergence of the matrix element is ensured by the Kinoshita–Lee–Nauenberg (KLN) theorem [13]. In the case of the Higgs boson decay, this entails including $H \to b\bar{b}$, $H \to b\bar{b}g$, $H \to b\bar{b}gg$, $H \to b\bar{b}ggg$, etc. Including these

degenerate states in the power expansion, presented in the beginning of the section, yields:

$$\begin{aligned}|\mathcal{M}_{b\bar{b}}|^2 =&|\mathcal{M}^{(0)}_{b\bar{b}}|^2 \\ &+\alpha_s \left(|\mathcal{M}^{(0)}_{b\bar{b}g}|^2 + 2\,\mathrm{Re}\Big\{\mathcal{M}^{(1)}_{b\bar{b}}(\mathcal{M}^{(0)}_{b\bar{b}})^*\Big\}\right) \\ &+\alpha_s^2 \left(|\mathcal{M}^{(1)}_{b\bar{b}}|^2 + |\mathcal{M}^{(0)}_{b\bar{b}gg}|^2 + 2\,\mathrm{Re}\Big\{\mathcal{M}^{(1)}_{b\bar{b}g}(\mathcal{M}^{(0)}_{b\bar{b}g})^*\Big\} + 2\,\mathrm{Re}\Big\{\mathcal{M}^{(2)}_{b\bar{b}}(\mathcal{M}^{(0)}_{b\bar{b}})^*\Big\}\right) \\ &+\dots\,.\end{aligned}$$

To summarise, the importance of KLN theorem lies in the fact that it ensures convergence at each order. That is, convergence does not come from adding terms at all orders, but from adding all relevant terms at each order. This is rather useful as it allows for computation of matrix element at some fixed order and provides a method for cancelling possible IR divergences.

2.3 Arguments for convergence

In this subsection we investigate the convergence of the virtual-real interference term. To do that, we study the propagators labelled in Figure 5.

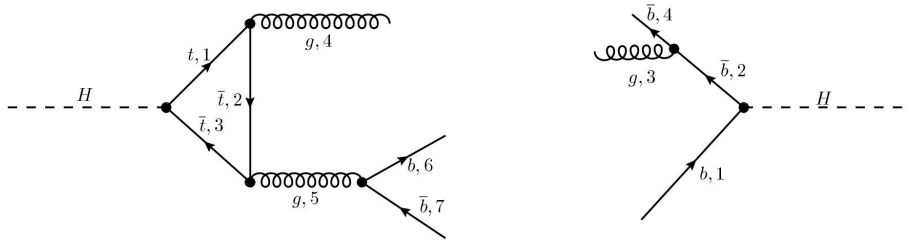

Figure 5: Virtual-real interference term with labels for each propagator.

Starting with the amplitude of the top-quark loop, the amplitude is proportional to the product of the propagators in the loop, as shown below:

$$\int \frac{\mathrm{d}^4 p_1\, N(p_1, p_b, p_{\bar{b}}, p_g)}{p_1^2 - m_t^2} \cdot \frac{1}{(p_1 - p_g)^2 - m_t^2} \cdot \frac{1}{(p_1 - p_g - (p_b + p_{\bar{b}}))^2 - m_t^2}, \tag{8}$$

where p_1 is the top quark's 4-momentum, and the function $N(p_1, p_b, p_{\bar{b}}, p_g)$ in the numerator is a general factor coming from the Feynman rules. The integral in Eq.(8) is due to the fact that there are no restrictions on the top quark's momentum [12]. We notice as well that the expression has no IR divergences because even if all the momenta cancels, the mass of the top is not 0. Thus, the propagators in the top-quark loop do not lead to divergences.
The amplitude of propagator (5) in the left diagram is proportional to:

$$\begin{aligned}\mathcal{A}^{(5)} \propto \frac{1}{Q^2} &= \frac{1}{(p_b + p_{\bar{b}})^2} \\ &= \frac{1}{p_b^2 + p_{\bar{b}}^2 + 2p_b \cdot p_{\bar{b}}} \\ &= \frac{1}{2m_b^2 + 2E_b E_{\bar{b}} + 2|\vec{p_b}||\vec{p_{\bar{b}}}|\cos\theta_{b,\bar{b}}}.\end{aligned} \tag{9}$$

Eq.(9) shows that the denominator is free of divergences for massive bottom quarks.
In the diagram to the right of Figure 5, we look at propagator (2). The amplitude for this propagator is proportional to:

$$\begin{aligned}\mathcal{A}^{(1)} \propto \frac{1}{Q^2 - m_b^2} &= \frac{1}{(p_{\bar{b}} - p_g)^2 - m_b^2} \\ &= \frac{1}{\cancelto{0}{p_g^2} + p_{\bar{b}}^2 - 2p_{\bar{b}} \cdot p_g - m_b^2} \\ &= \frac{1}{-2E_g(E_{\bar{b}} - |\vec{p_{\bar{b}}}| \cos\theta_{g,\bar{b}})},\end{aligned} \tag{10}$$

where the last fraction could contain divergences if the gluon was soft or if the anti-bottom quark was massless and collinear to the gluon. This infinity can be cancelled because of the diagram to the left in Figure 5. More specifically, we note that the propagator for gluons given in Eq.(9) contains a factor, which was omitted. In particular, it can be shown that this factor is proportional to:

$$p_{g,4} \cdot (p_b + p_{\bar{b}}) g^{\mu\nu} - p_{g,4}^{\mu}(p_{\bar{b}}^{\nu} + p_b^{\nu}), \tag{11}$$

where $g^{\mu\nu}$ is the metric tensor, and p_i^{ν} is the component of the 4-momentum of the i particle. Eq.(11) shows that if the gluon's momentum is 0, then the whole numerator would go to 0 linearly, as does the denominator in Eq.(10). This means that as the gluon's momentum goes to 0, the interference term:

$$\mathrm{Re}\Big\{\mathcal{M}_{b\bar{b}g}^{(1)}(\mathcal{M}_{b\bar{b}g}^{(0)})^*\Big\} \tag{12}$$

$$\underbrace{\mathcal{M}_{b\bar{b}g}^{(1)}}_{\longrightarrow 0}\underbrace{(\mathcal{M}_{b\bar{b}g}^{(0)})^*}_{\longrightarrow \infty} \approx C, \tag{13}$$

goes to some constant C. Thus, the interference term is finite.

With these arguments, we conclude that the contribution of interest has no IR divergences, and it is then finite on its own.

3 Methods

For the purposes of this thesis, MadGraph5_aMC@NLO was used. MadGraph5_aMC@NLO (MG) [14] is a Monte Carlo based event generator that can be used to calculate decay rates, and cross sections, among others. In the following, we give an outline of how MG works in general, as well as how it is used in this project.

To explain the basic principles MG is based on, consider a function $f(x)$, such as the one shown in Figure 6.

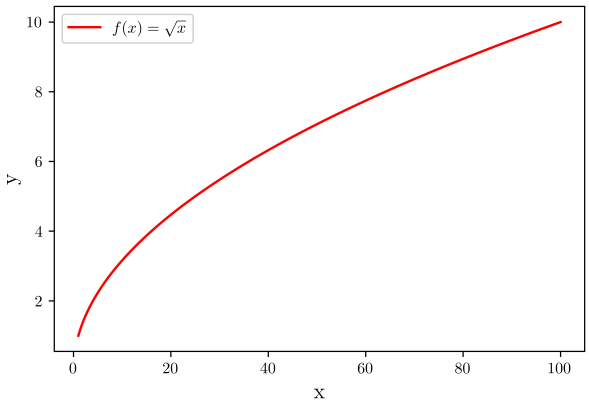

Figure 6: Plot of $f(x) = \sqrt{x}$.

The issue we are concerned with is finding the integral of $f(x)$ in the interval $[x_1, x_2]$ - for the example depicted it would be from $[1, 100]$. The Monte Carlo method consists of evaluating the function at some randomly chosen points, x_i, and then taking the average of these. Mathematically,

$$I = \int_{x_1}^{x_2} \mathrm{d}x f(x) \approx (x_2 - x_1) \frac{1}{N} \sum_{i=0}^{N} f(x_i). \tag{14}$$

In the context of particle physics, $f(x)$ would correspond to the matrix element squared, $\mathcal{M}^2$, which is integrated over the phase-space of the final state particles.
This means that the data obtained from simulations, or the randomly selected points to continue with the example, are events. In each of these events, the final state particles - b, $\bar{b}$, g - have a specific momentum which is contained in the event file.

As explained in Ref. [15], Effective field theories (EFT's) describe only relevant phenomena within a certain energy scale or regime, neglecting other effects that do not play a role. In general, these theories can serve to build the bigger, perhaps unknown, theory. This approach is known as bottom-up view. EFT's are also relevant in other cases when it may be useful to construct a simpler theory even if the bigger, underlying theory is known. Practically, this entails making simplifications to the bigger theory, thereby possibly reducing the computational complexity of the calculations performed within that regime [15]. This is known as top-down approach.

This approach is used in Higgs Effective Field Theory (HEFT). HEFT is used in this paper, since MG can only calculate decay rates of processes that can be drawn as a tree-level Feynman diagram. As the contribution of interest contains a top-quark loop, we need to transform it into a single vertex with an effective coupling. For this we make use of HEFT.

In this paper, the goal is to calculate the decay rate of the specific interference contribution shown in Figure 1a.
Firstly, the model `heft` has to be imported to replace the top loop by an effective coupling between the Higgs boson and gluons known as *HIG*. To specify the contribution in MG, the following syntax was used:
`generate h > b b~ g QCD^2==2 QED^2==1 HIG^2==1`,
where `^2` specifies that the term of interest is in the expansion of the matrix element squared, and the different coupling constants - `QCD, QED, HIG` - are used to determine all the vertices that identify the specific real-virtual interference. In this way, `QCD^2==2`

comes from the two gluon-bottom vertex, `QED^2==1`, which corresponds to the Yukawa vertex between the Higgs boson and the bottom quark pair, and `HIG^2==1`, which specifies the vertex of the effective Higgs to gluon coupling (See Figure 7).

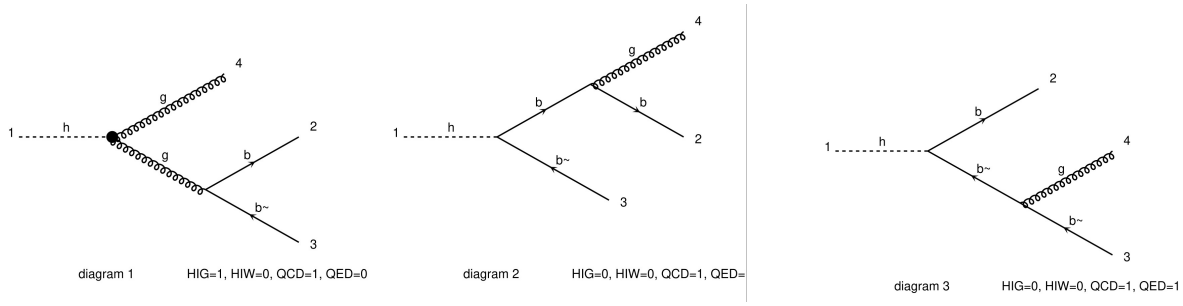

(a) **(b)**

Figure 7: Feynman diagrams taken from MG showing the relevant couplings for determining the interference of interest.

To calculate the LO term, one can simply use the following syntax:
`generate h > b b~`,
this evaluates the simplest Feynman diagram.

4 Results

For the simulation of the Higgs boson decay, 10000 events were generated using the syntax presented in the previous section. In this section, the simulation will be analysed to ascertain the convergence and size of the contribution. The code used to make the plots is available upon request.

4.1 On convergence

Firstly, in order to show that the contribution is finite, the ratio of the magnitude of the momentum of the different particles is plotted as a histogram. Figure 8 shows the ratio between the magnitude of the momentum of g over b. This plot indicates that the momentum of the gluon is not necessarily smaller than anti-bottom quark's momentum. More precisely, the decay rate does not diverge as the gluon's momentum approaches 0. This means that in Eq.(13), the constant would take the value 0. In other words, the contribution is finite.

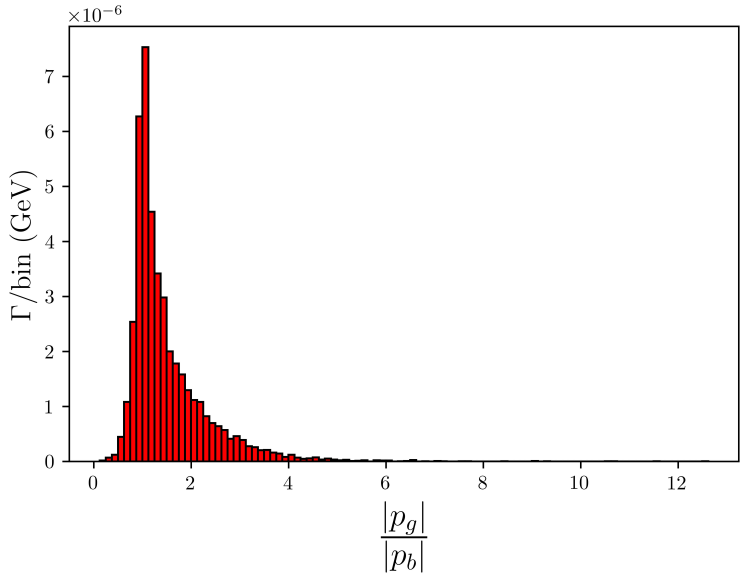

Figure 8: Decay width as a function of the ratio of the magnitude of the momentum of g and b.

4.2 Size of the contribution

Using the syntax described earlier, the integrated decay rate for the contribution of interest was found to be $4.4 \cdot 10^{-5}$ GeV. Whereas the total decay rate for the leading order term $H \to b\bar{b}$, was $5.4 \cdot 10^{-3}$ GeV. Thus, the contribution of interest changes the decay rate of the Higgs boson by 0.8%. As shown in Table 5 in Ref. [16], the branching ratio of $H \to b\bar{b}$ is known with an uncertainty of 0.2%. Thus, the contribution here presented is not negligible.

The uncertainties of these values are not presented in this thesis, but it should be noted that they are not dependent on the number of events generated.

4.3 Phase-space analysis

To analyse the phase space of the decay particles, namely $b\bar{b}g$, the data will be plotted in two different ways. Firstly, using Dalitz plots, and then by plotting the angle between the decay particles.

4.3.1 Dalitz plot

A common type of plot used to visualise the phase-space of the decay products, particularly for three-body decay, is the Dalitz plot.
In three-body decays, this type of plot shows the relation between m_{12}^2, m_{23}^2, and m_{13}^2. This serves as an illustration for how particles are correlated after the decay happened. To see this, we first expand each of the squared masses:

$$m_{12}^2 = (p_1 + p_2)^2 = (p - p_3)^2 = M^2 + m_3^2 - 2ME_3 \tag{15}$$
$$m_{23}^2 = (p_2 + p_3)^2 = (p - p_1)^2 = M^2 + m_1^2 - 2ME_1 \tag{16}$$
$$m_{13}^2 = (p_1 + p_3)^2 = (p - p_2)^2 = M^2 + m_2^2 - 2ME_2, \tag{17}$$

where the second equality comes from requiring momentum conservation, that is $p = p_1 + p_2 + p_3$ with $p = (M, \vec{0})$.

Eqs.(15)-(17) show that, for example, the maximum in m^2_{13} happens when particle 2 is at rest. In this case, by momentum conservation, particles 1 and 3 would have the same momentum in magnitude but opposite in direction. Similarly, the maximum in m^2_{12} occurs when the third particle is at rest. In such case, particles 1 and 2 are moving opposite direction, meaning that the angle between them is π.
In summary, each point in the Dalitz plot can be mapped to a specific configuration of the momenta of the three particles.
Another relevant point to make is that an inhomogeneous distribution of points in the Dalitz plot indicates the most common configuration of the particles after the decay happened.
Figure 9, shows the Dalitz plot for the contribution of interest. The density of points in the plot does not seem uniform indicating that the most likely configurations are: either the bottom quark is very soft and $\bar{b}$ and g have the same but oppposite momentum or $\bar{b}$ is very soft and the momentum is equally distributed between b and g.

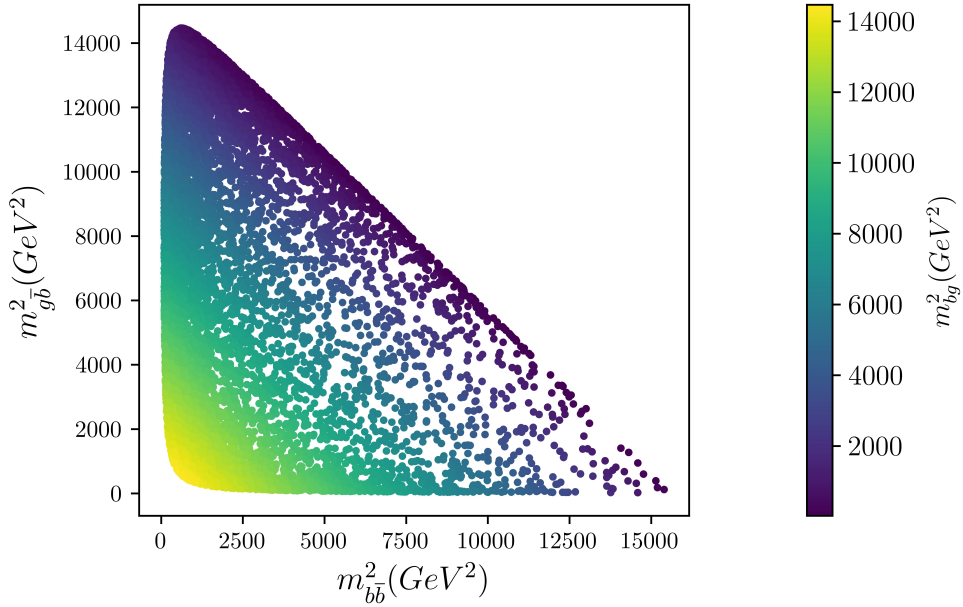

Figure 9: Dalitz plot for Higgs boson decay. On the x-axis $m^2_{b\bar{b}}$, on the y-axis $m^2_{g\bar{b}}$ and the colour-bar shows m^2_{bg} in GeV^2.

From this we see that, on average, the gluon's momentum is not in the soft energy regime.

4.3.2 Angular distributions

Plotting the angle between the particles also serves to reveal the particle's direction and momentum after the decay.
We expect the histogram of the angle between b and g to have a similar shape to the plot of the angle between $\bar{b}$ and g, as the gluon can be emitted from either b or $\bar{b}$ without particular preference. Also, from the preceding subsection about the Dalitz plot, we expect the angle b and g to peak around π.
Figures 10 and 11 show that the histograms have a similar shape suggesting that there

is no preference for the gluon being emitted from either of the bottom quarks, as it was expected.

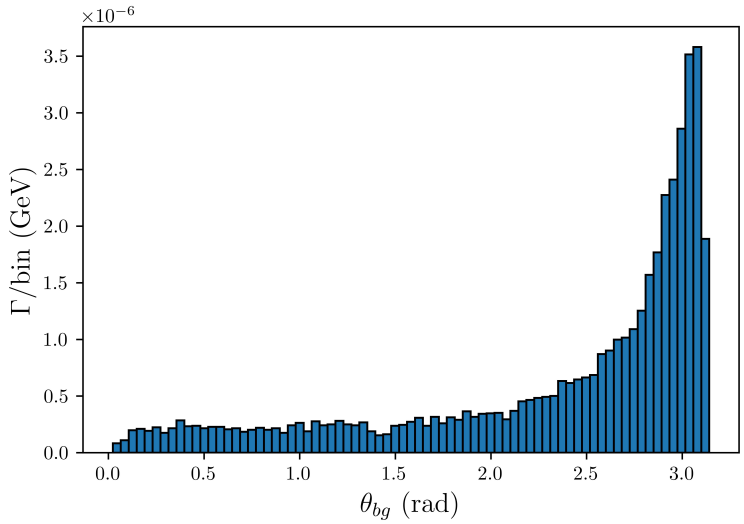

Figure 10: Decay width as a function of the angle between b and g in radians.

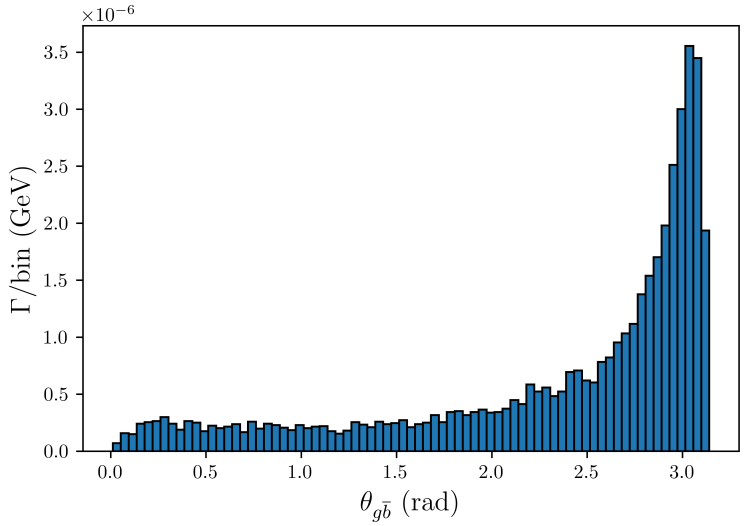

Figure 11: Decay width as a function of the angle between g and $\bar{b}$ in radians.

Figure 12 shows a more homogeneous distribution of angles. That is, there is no particular preference for one angle, as opposed to the previous plots where there was a clear peak at around π. The reason for this is that in most cases either the bottom quark or the anti-bottom quark is soft, and the other one is hard. In other words, the angle of the soft quark is arbitrary because its momentum is negligible compared to the other particles' momenta.

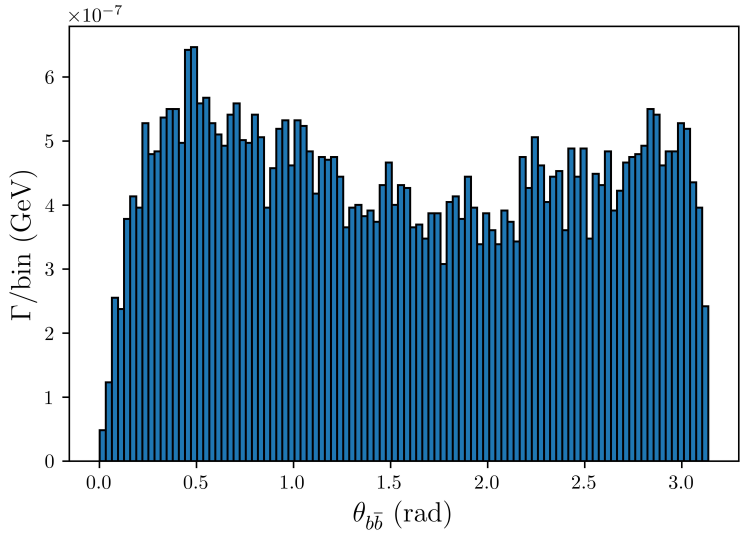

Figure 12: Histogram showing the angle between b and $\bar{b}$ in radians.

5 Conclusion

In this thesis the main focus was to study an interference term of Higgs boson decay to $b\bar{b}$ at next-to-next-to-leading order in the perturbative expansion in α_s. We have shown that this term is indeed finite on its own and, using MG to simulate the decay, we have computed how large this contribution is compared to the leading order and concluded from this that the term is not negligible.
Some of the possible ways of extending this work may involve taking into account Higgs boson production to the computation of the decay rate, study how possible uncertainties might affect results here presented, and or, studying the other NNLO interference term including a double virtual loop (see Figure 1b).

Acknowledgements

I would like to thank my supervisor, Rikkert Frederix, for answering all my questions with very clear explanations, for the invaluable feedback and for the constant patience.
I am also grateful to Nils Schneider for letting me organise my thoughts with you and for all the emotional support. Thank you.

References

[1] Peter W. Higgs. "Broken Symmetries and the Masses of Gauge Bosons". In: *Phys. Rev. Lett.* 13 (1964). Ed. by J. C. Taylor, pp. 508–509. DOI: 10.1103/PhysRevLett.13.508.

[2] F. Englert and R. Brout. "Broken Symmetry and the Mass of Gauge Vector Mesons". In: *Phys. Rev. Lett.* 13 (1964). Ed. by J. C. Taylor, pp. 321–323. DOI: 10.1103/PhysRevLett.13.321.

[3] Serguei Chatrchyan et al. "Observation of a New Boson at a Mass of 125 GeV with the CMS Experiment at the LHC". In: *Phys. Lett. B* 716 (2012), pp. 30–61. DOI: 10.1016/j.physletb.2012.08.021. arXiv: 1207.7235 [hep-ex].

[4] Georges Aad et al. "Observation of a new particle in the search for the Standard Model Higgs boson with the ATLAS detector at the LHC". In: *Phys. Lett. B* 716 (2012), pp. 1–29. DOI: 10.1016/j.physletb.2012.08.020. arXiv: 1207.7214 [hep-ex].

[5] Vittorio Del Duca et al. "Higgs boson decay into b-quarks at NNLO accuracy". In: *JHEP* 04 (2015), p. 036. DOI: 10.1007/JHEP04(2015)036. arXiv: 1501.07226 [hep-ph].

[6] Fabrizio Caola et al. "NNLO QCD corrections to associated WH production and $H \to b\bar{b}$ decay". In: *Phys. Rev. D* 97.7 (2018), p. 074022. DOI: 10.1103/PhysRevD.97.074022. arXiv: 1712.06954 [hep-ph].

[7] Arnd Behring and Wojciech Bizoń. "Higgs decay into massive b-quarks at NNLO QCD in the nested soft-collinear subtraction scheme". In: *JHEP* 01 (2020), p. 189. DOI: 10.1007/JHEP01(2020)189. arXiv: 1911.11524 [hep-ph].

[8] Amedeo Primo et al. "Exact Top Yukawa corrections to Higgs boson decay into bottom quarks". In: *Phys. Rev. D* 99.5 (2019), p. 054013. DOI: 10.1103/PhysRevD.99.054013. arXiv: 1812.07811 [hep-ph].

[9] David J. Griffiths. *Introduction to elementary particles*. 2., rev. ed., 5. reprint. Physics textbook. Weinheim: Wiley-VCH, 2011. 454 pp. ISBN: 978-3-527-40601-2.

[10] Michael Edward Peskin and Daniel V. Schroeder. *An introduction to quantum field theory*. The advanced book program. Boca Raton London New York: CRC Press, Taylor & Francis Group, 2019. 842 pp. ISBN: 978-0-367-32056-0 978-0-201-50397-5.

[11] Günther Dissertori, I. G. Knowles, and Michael Schmelling. *Quantum chromodynamics: high energy experiments and theory*. OCLC: 1058384333. Oxford: Oxford University Press, 2009. ISBN: 978-0-19-170806-0.

[12] Robert D. Klauber. *Student friendly quantum field theory. volume 1: Basic principles and quantum electrodynamics / Robert Klauber*. Second edition (fourth revision with improvements and corrections). Fairfield, Iowa: Sandtrove Press, 2022. 527 pp. ISBN: 978-0-9845139-5-6 978-0-9845139-4-9.

[13] Taizō Muta. *Foundations of quantum chromodynamics: an introduction to perturbative methods in gauge theories*. World Scientific lecture notes in physics 5. Singapore: World Scientific, 1987. ISBN: 978-9971-950-40-8.

[14] J. Alwall et al. "The automated computation of tree-level and next-to-leading order differential cross sections, and their matching to parton shower simulations". In: *JHEP* 07 (2014), p. 079. DOI: 10.1007/JHEP07(2014)079. arXiv: 1405.0301 [hep-ph].

[15] Johann Brehmer. "Higgs Effective Field Theory". Short Lectures for the Heidelberg RGT. 2016. URL: https://www.thphys.uni-heidelberg.de/~gk_ppbsm/lib/exe/fetch.php?media=students:lectures:student_lecture_eft.pdf.

[16] Michael Spira. "Higgs Boson Production and Decay at Hadron Colliders". In: *Prog. Part. Nucl. Phys.* 95 (2017), pp. 98–159. DOI: 10.1016/j.ppnp.2017.04.001. arXiv: 1612.07651 [hep-ph].